RSC Advances

This is an *Accepted Manuscript*, which has been through the Royal Society of Chemistry peer review process and has been accepted for publication.

Accepted Manuscripts are published online shortly after acceptance, before technical editing, formatting and proof reading. Using this free service, authors can make their results available to the community, in citable form, before we publish the edited article. This *Accepted Manuscript* will be replaced by the edited, formatted and paginated article as soon as this is available.

You can find more information about *Accepted Manuscripts* in the Information for Authors.

Please note that technical editing may introduce minor changes to the text and/or graphics, which may alter content. The journal's standard Terms & Conditions and the Ethical guidelines still apply. In no event shall the Royal Society of Chemistry be held responsible for any errors or omissions in this *Accepted Manuscript* or any consequences arising from the use of any information it contains.

ROYAL SOCIETY OF CHEMISTRY

www.rsc.org/advances

Please do not adjust margins

RSC Advances

ARTICLE

Morphological and structural characterisation of sol-gel electrospun Co_3O_4 nanofibres and their electro-catalytic behaviour

Received 00th January 20xx,
Accepted 00th January 20xx

DOI: 10.1039/x0xx00000x

www.rsc.org/

Gibin George[a], Liju Elias[b], A. Chitharanjan Hegde[b] and S. Anandhan[a]*

Evolution of hydrogen and oxygen are a crucial part of many renewable energy systems. The replacement of the essential and expensive components in such systems can reduce the capital cost and improve the effectiveness of those systems. In this study, Co_3O_4 nanofibres were fabricated from sol-gel assisted electrospun poly(styrene-*co*-acrylonitrile)/cobalt acetate tetrahydrate precursor composite fibres. The morphological and compositional features of the Co_3O_4 nanofibres obtained after calcination of the precursor nanofibers were studied using scanning electron microscopy, transmission electron microscopy, X-ray photoelectron spectroscopy and Fourier transform infrared spectroscopy. The results of X- ray diffraction study and Raman spectroscopy revealed that the average grain size composing the fibres increased with the calcination temperature. A clear evidence of defects in the fibres was observed in ultraviolet-visible-near infrared and energy dispersive spectroscopic measurements. The electrocatalytic behaviour of Co_3O_4 nanofibres obtained at different calcination temperatures was studied using them for water splitting reaction in an alkaline medium. The maximum efficiency in hydrogen evolution reaction was achieved using the Co_3O_4 nanofibres obtained at the lowest calcination temperature, which had the highest surface area and the smallest grain size.

Introduction

Hydrogen is emphatically considered as a potential renewable energy source, as it not only has high energy content per unit mass but also does not produce any environmentally malignant molecular species during its combustion. Hydrogen has been used as a fuel in proton exchange membrane fuel cells (PEMFC) with high energy conversion efficiencies. The oxygen evolution reaction is of great importance in the fields of energy production (water electrolysis) and electro synthesis (electrometallurgy in aqueous media).[1]

In electrocatalysis, hydrogen evolution reaction (HER) and oxygen evolution reaction (OER) are two important electrochemical processes in connection with water electrolysis, or fuel cell applications. Many oxide nanomaterials have widely been replacing the expensive precious metal components of PEMFC, especially the electrodes, to reduce the capital cost of them. Other than noble metals, metals like cobalt, nickel, iron are also useful in the evolution of H_2 and O_2, but they are unstable at their low valance states, where the hydrogen production is significant.[2] Also, the high overpotentials of them for HER can hinder the large scale hydrogen production. These factors necessitated the development of advanced electrode materials, having low electrode polarization with better electrocatalytic efficiency.[3] Similarly, a drastic change in polarization conditions is preferred for OER, which can be achieved by developing efficient electroactive catalysts, which can show optimal performance. Cost effective and active nanosized semiconducting metal oxides are potential candidates for HER and OER, because, they are more stable than the parent metals. Moreover, their high surface area and the presence of crystal defects can favour the water splitting reactions.

Oxide nanomaterials are unique and they have several advanced applications starting from an electronic component used in MEMS devices to dispersion in coolant for internal combustion engines. The morphology and aspect ratio of the oxide nanomaterials are not important for several applications, where size effects play a major role; but, in some specific applications, such as sensors, dye sensitized solar cells (DSSCs) and field-effect transistors (FETs),[4] where the continuous electron transport is essential, the morphology and aspect ratio are important. Nanofibres can perform better than nanoparticles in such applications. Producing a high aspect ratio nanomaterial is challenging, especially, when one of its dimensions is close to macroscale. In conventional chemical synthesis, aligned fibres can be fabricated within the microscale, but, the process is tedious, time consuming and

[a] Department of Metallurgical and Materials Engineering.
[b] Electrochemistry Research Laboratory, Department of Chemistry.
National Institute of Technology-Karnataka, Srinivas Nagar, Mangaluru-575025, India. E-mail: anandtmg@gmail.com; anandhan@nitk.edu.in; Fax: +91-824-2474059; Tel: +91-824-2473762

†Electronic Supplementary Information (ESI) available: See DOI: 10.1039/x0xx00000x

RSC Advances Accepted Manuscript

requires ultrapure precursors that will ultimately lead to high production costs. To overcome these difficulties associated with the conventional processing of ceramic nanofibres, sol-gel assisted electrospinning process is a better option.

Electrospinning is a simple and scalable technique for the production of polymer and ceramic nanofibres. Sol-gel technique has been used as preliminary step for the preparation of a spinnable sol, followed by electrospinning of sol-gel to xerogel fibres and then calcination at an appropriate temperature. While preparing a spinnable sol, a metal salt of the corresponding metal oxide, a polymer solution in a suitable solvent with adequate viscosity is mixed together at molecular level. The metal salt/polymer xerogel fibres are fabricated at optimized spinning conditions. The xerogel fibres are then calcined above the degradation temperature of the polymer and the metal salt so as to get the metal oxide nanofibres.[5]

The applications of 1D nanofibrous oxide materials are vast and a large number of metal oxides nanofibres have been fabricated from simple oxide to complex and composite oxides. Many oxide nanomaterials and their derivatives are used in the water splitting reactions. For instance, the common oxide nanomaterials, such as, TiO_2,[6,7] ZnO,[8] Fe_2O_3,[9] etc. are used as electrodes for photoelectrocatalytic hydrogen evolution. Nanoparticles of rare earth metal oxides IrO_2 and RuO_2 are also potential candidates for the water splitting reactions.[10] Photoelectrocatalytic water splitting can have several drawbacks of which the major one is the requirement of light. Similarly, the use of rare earth oxides is limited by their scarcity and high cost. The metal oxides with the metal cations in the higher oxidation states can perform better in OER.[11]

When cobalt oxide is used as a working electrode for alkaline water splitting, the oxidation of Co^{3+} to Co^{4+} under applied electric field favours OER since the Co^{4+} ions can in turn act as active sites for adsorption of OH^- during OER from alkaline solution. Whereas, the reduction of Co^{3+} to Co^{2+} in a basic medium when the Co_3O_4 is connected as an cathode is favourable for HER since it can favour the adsorption of H^+. Therefore, cobalt oxide can be used as an electrocatalyst for HER and OER simultaneously. The high surface area of the Co_3O_4 nanofibres, the presence of crystal defects and continuous electron transport can significantly contribute to the electrocatalytic activity in electrospun Co_3O_4 nanofibres. There are reports on electrocatalytic activity of mixed oxides containing cobalt oxide in different valence states for overcoming the problem of oxygen overpotential.[12]

The electrocatalytic activity of a material depends markedly on the chemical and phase composition, geometric properties and structure of the electrode surface. The electrolysis of aqueous alkaline hydroxide solutions is one of the most popular routes for the production of hydrogen and oxygen from water. In this study, Co_3O_4 nanofibres were fabricated by calcination of electrospun composite fibres of poly(styrene-*co*-acrylonitrile)(SAN)/cobalt acetate tetrahydrate (CATH). The interaction between the nitrile group of SAN and the carbonyl group of cobalt acetate assures the uniform dispersion of metal salt in the polymer solution.[13] The bulky styrene side groups of SAN can act as a framework for the conversion of composite fibres to ceramic fibres. The structural characteristics of Co_3O_4 nanofibres prepared by the sol-gel assisted electrospinning were characterized by different techniques. The electrocatalytic property of Co_3O_4 nanofibres were evaluated by using them for the water splitting to HER and OER in alkaline solution.

Materials and methods

SAN [Grade: Santron IMS 1000, acrylonitrile content: 30%, specific gravity: 1.07, $\overline{M}_v$: 2.46×10^6 (viscometry), MFI: 35 g/10 min at 220 °C under a load of 10 kg, ASTM D-1238] obtained from Bhansali Engineering Polymers, Rajasthan, India, cobalt (II) acetate tetrahydrate ($Co(OCOCH_3)_2.4H_2O$, assay 98%) (CATH) procured from High Purity Laboratory Chemicals, Mumbai, India and N, N-dimethyl formamide (DMF, assay>99%) purchased from Sisco Research Laboratories Pvt. Ltd, Mumbai, India, were used without further purification to fabricate the precursor composite fibres.

To prepare the spinnable sol, 2 g of SAN was dissolved in 10 mL of DMF in a stoppered glass vial by continuous stirring for 4 hours and 2 g of CATH were added into it. The mixture was stirred vigorously for 6 h to ensure the uniform mixing of CATH in SAN solution and this mixture formed a spinnable sol. The ratio between SAN and CATH was maintained as 1:1 in this study.

The precursor composite fibres of SAN/CATH were fabricated by electrospinning process. The sol prepared in the previous step was loaded to a 10 mL syringe attached with a hypodermic needle [inner diameter: 0.5 mm and outer diameter: 0.8 mm] chamfered at the tip. The syringe with the sol was loaded to a vertical electrospinning unit (E-Spin Nano, Physics Equipments Co., Chennai, India) and the needle was connected to a +ve DC potential. The fibres were collected on a grounded metallic collector plate covered with an aluminium foil. The applied voltage was varied as 15, 17, 20 and 22 kV to obtain the minimum fibre diameter and a maximum yield. Optimum electrospinning conditions reported for SAN in literature were used, the tip-to-collector distance was 17 cm and the solution flow rate was 1000 μL h^{-1}.[14]

The SAN/CATH composite fibre mat that was peeled off the aluminium foil was calcined in a programmable high temperature furnace (Indfur, Chennai, India) to obtain Co_3O_4 nanofibres. The heating rate was adjusted to 4 K.min^{-1} and the calcination temperature was varied as 773, 873 and 973 K, the dwell period was fixed as 2 hours. The minimum calcination temperature was based on the degradation temperature of the SAN/CATH composite fibres during their thermogravimetric analysis (TGA) (EXSTAR 6000 TG/DTA 6300, Japan) in a nitrogen atmosphere at a heating rate of 10 K min^{-1}.

A scanning electron microscope (SEM) (JEOL JSM-6380LA, Japan) was utilized to examine the morphology of the electrospun fibres before and after calcination. An energy dispersive X-ray spectroscope (EDS) (Link ISIS-300 Micro-analytical System, Oxford Instruments, UK) attached to the

RSC Advances Accepted Manuscript

 This journal is © The Royal Society of Chemistry 20xx

SEM was used for analysing the composition of the ceramic fibres. The gold sputtered samples (sputtered by JFC 1600 autofine coater EOL, Japan) were analysed in SEM and their diameters were measured using an image processing and analysis program, ImageJ[15]. Transmission electron micrographs (S-5500, Hitachi, Japan) and the SAED pattern were used to identify the finer morphology of the fibres. Fourier transform infrared (FTIR) spectra (Jasco FTIR-4200, Japan) of SAN, CATH, precursor composite and the calcined fibres were recorded in transmission mode by the KBr pellet method in a wave number range of 400-4000 cm^{-1} for an average of 32 scans. X-ray diffraction patterns (XRD) (JEOL X-ray diffractometer, DX-GE-2P, Japan) were obtained using CuK_α radiation within a 2θ range of 10°-80º, at a scanning rate of 0.5 ºmin^{-1}. UV-Vis-NIR spectra (Varian, Cary 5000 UV-Vis-NIR, USA) of the ceramic fibres were recorded in the diffused reflectance mode in the wavelength range of 215-2400 nm. Micro Raman spectra (inVia, Renishaw, UK) were collected for the cobalt oxide samples prepared at different calcination temperatures, in the wave number range of 60-2000 cm^{-1} using an Argon ion laser source with a power of 100 mW and a wavelength of 514 nm. X-ray photoelectron spectra (XPS) were recorded at 25 °C, using monochromated Al K_α radiation (15 keV) for excitation (Axis 165, X-ray Photoelectron Spectrometer, Kratos Analytical, UK) and a spherical mirror analyzer. Specific surface area values of the Co_3O_4 nanofibres were measured by the BET method, after degassing the samples for 6 h at 150 °C (Smart sorb 92/93, Smart Instruments Co. Pvt. Ltd, Dombivli, India) under a high vacuum.

The electrodes for HER and OER were prepared on cylindrical graphite rods of 10 mm diameter. Graphite rod was polished at one end and the sides were sealed with a Teflon tape. Then, the electrode was sonicated for half an hour in DI water and then dried. 10 mg/mL suspension of Co_3O_4 nanofibres was prepared in ethanol by sonication and 1 mL of this solution was dropped onto the polished end of the graphite electrode. After drying in air, 20 µL of a 0.5% solution of poly(vinylidene fluride) (PVDF) in acetone was also dropped on the Co_3O_4 nanofibrous layer to keep the Co_3O_4 nanofibres in position. The electrodes were prepared from Co_3O_4 nanofibres calcined at 773, 873 and 973 K. These electrodes were soaked in 1 M KOH for one hour to attain the equilibrium before HER and OER studies. The PVDF loaded graphite electrode was also prepared (bare) as a control.

The alkaline water splitting efficiency of electrospun cobalt oxide nanofibres calcined at different temperatures (773, 873 and 973 K) were studied in 1 M KOH solution using cyclic voltammetry and chrono-potentiometry methods. All electro-catalytic study of electrospun cobalt oxide nanofibre modified graphite electrode was carried out in a home-made three-electrode tubular glass cell as shown in Fig. 1. The electrocatalytic study set up was designed in such way to have the provision for collecting the evolved H_2 and O_2 during electrolysis. This allows in relating the amount of gas liberated at a given time with the characteristics of the electrode materials calcined at different temperatures. The electrocatalytic study was carried out using the modified graphite electrode with an effective surface area of $1cm^2$ as the working electrode and the platinised platinum of same surface area (1.0 cm^2) as the counter electrode. A saturated calomel electrode (SCE) was used as the reference electrode through a Luggin's capillary with Agar-KCl salt bridge, to eliminate the error due to Ohmic drop. The modified graphite electrodes were subjected to cyclic voltammetry (CV) and chrono-potentiometry study under 1 M KOH medium, using computer controlled Potentiostat/Galvanostat (Biologic SP-150, Biologic Science Instruments, France) to analyse its electrochemical behaviour in terms of HER and OER.

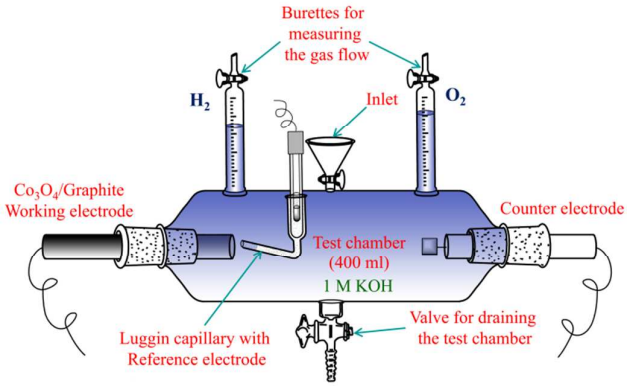

Fig. 1 Test setup used for the hydrogen and oxygen evolution studies.

Results and discussion

Characterization of precursor composite fibres

Randomly oriented bead-free precursor fibres were obtained as seen in the SEM images of the precursor fibres (Fig. S1, ESI†). As the applied voltage was increased, the average fibre diameter (AFD), coefficient of fibre uniformity (C_{FU}) (Eqns S1 & S2, ESI†) and the standard deviation of fibre diameter decreased and a minimum was obtained at an applied voltage of 22 kV (Table S1, ESI†). When the applied voltage was increased above 22 kV, thinner fibres were obtained; but, the amount of fibres collected on the collector plate was less, since a substantial amount of fibres were collected at several charged points in the electrospinning chamber. Therefore, 22 kV was considered to be the optimum voltage for the fabrication of the SAN/CATH composite fibres (Fig. 2a). When the applied voltage was changed, the number of charges accumulated at the liquid jet surface also changed. Therefore, as the applied voltage was increased more charges got accumulated at the droplet surface, which resulted in thin fibres due to quicker drawing of the jet.

To find the appropriate calcination temperature of these composite fibres to obtain pure Co_3O_4 nanofibres, TG analysis was carried out and the TG and derivative thermogravimetric (DTG) plots of SAN and SAN/CATH composite fibres are shown in Fig. 2b. SAN exhibits a single step and SAN/CATH composite exhibits three step degradation. The onset of degradation for SAN is 663 K and the degradation ended at 773 K. In the case of SAN/CATH composite, the weight loss step at 473 K is due to the evolution of water from CATH. The severe degradation of

RSC Advances Accepted Manuscript

SAN in presence of CATH is due to the release of acetic acid from CATH as shown in Eqn. S3 (ESI†), which catalyses the degradation of SAN.[16] The third step is due to the concurrent conversion of CoO and $CoCO_3$ to Co_3O_4.[17] The overall transition of CATH to Co_3O_4 is briefed as Eqns S3-S6 (ESI†, section 2).

The interaction between SAN and CATH determines their mutual miscibility/compatibility. FTIR spectrum is used to ascertain the interaction between SAN and CATH. Fig. 2c shows the FTIR spectra of SAN/CATH composites and SAN/CATH composite fibres after heating at 423 K for twelve hours. The peak assignments are presented in supplementary information (ESI†, section 3).

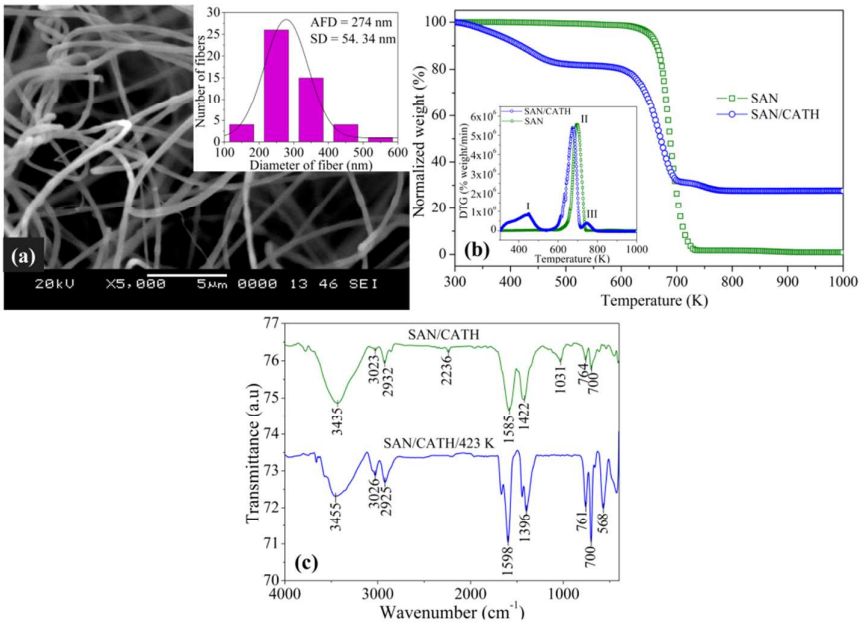

Fig. 2 (a) SEM micrographs (histogram in the inset), (b) TG plots (DTG in the inset) and (c) FTIR spectra of SAN/CATH composite fibres.

The peaks in SAN/CATH composite are a combination of those of SAN and CATH. The peak at 1516 cm^{-1} of CATH, which corresponds to C=O stretching in ionized acetate is shifted to a higher wavenumber (1585 cm^{-1}) when it formed a composite with SAN. A remarkable reduction in the intensity of the peak at 2239 cm^{-1}, which corresponds to C≡N stretching, in SAN/CATH composite as compared with the pure SAN is also observed. Both these results confirm a good interaction between the nitrile group of SAN and the carbonyl group of CATH in the SAN/CATH precursor composite fibres, therefore a uniform mixing of CATH (Fig. S2, ESI†).

Once the SAN/CATH composite fibres are heated at 423 K for 12 hours, the peaks corresponding to the styrene groups are dominating over the other characteristic peaks (Fig. 2c). Hence, the ability of the styrene group to act as a structural element during the calcination process is also revealed with the help of FTIR spectral analysis.

Characterization of cobalt oxide (Co_3O_4) nanofibres

Fig. 3a-c shows the SEM images of randomly oriented Co_3O_4 nanofibres obtained at different calcination temperatures and the corresponding diameter histograms. Due to the removal of SAN and the organic part of CATH, AFD values of the ceramic fibres are lower than those of the SAN/CATH composite fibres. AFD of Co_3O_4 nanofibres decrease with an increase in the calcination temperature, which is attributed to the grain growth and densification of the fibres (Table 1). AFD, standard deviation and C_{FU} of the nanofibres at different calcination temperature were calculated and their values are presented in Table 1.

Table 1 AFD, SD and C_{FU} of Co_3O_4 nanofibres

Calcination temperature (K)	AFD (nm)	SD (nm)	CFU
773	126	30.1	1.17
873	101	28.3	1.12
973	95.9	24.5	1.10

TEM images of the Co_3O_4 nanofibres obtained at different calcination temperatures are shown in Fig. 4. The grains composing the fibres (Fig. 4 a & b) are revealed, when the samples were analysed after sonicating the fibres in ethanol. In all the figures, in the inset, the lattice fringes with the spacing corresponding to that of Co_3O_4 were obtained. Selected area electron diffraction (SAED) pattern (in the inset) confirms the formation of Co_3O_4 and the diffraction rings can be indexed to the planes of spinel structured Co_3O_4. In Fig. 4c, the TEM image of a single fibre obtained at 973 K is shown, which has its grains densely packed. For a dense packing, one can expect grains with polygonal shapes, whereas in the case of loosely packed structures grains with ellipsoidal or any other intricate shapes can be expected. Upon closer observation, in the case of fibres calcined at 773 K (Fig. 4a), the majority of grains with ellipsoidal and other shapes with soft edges can be seen. As

RSC Advances Accepted Manuscript

 This journal is © The Royal Society of Chemistry 20xx

the calcination temperature is increased to 873 K (Fig. 4b), the shapes of a number of grains are changed to polygonal as marked by the red arrows indicating the densification of grains with calcination temperature. Denser fibres are obtained at 973 K. The gaps between the grains in the fibres calcined at low temperatures can contribute to an increased surface area in them.

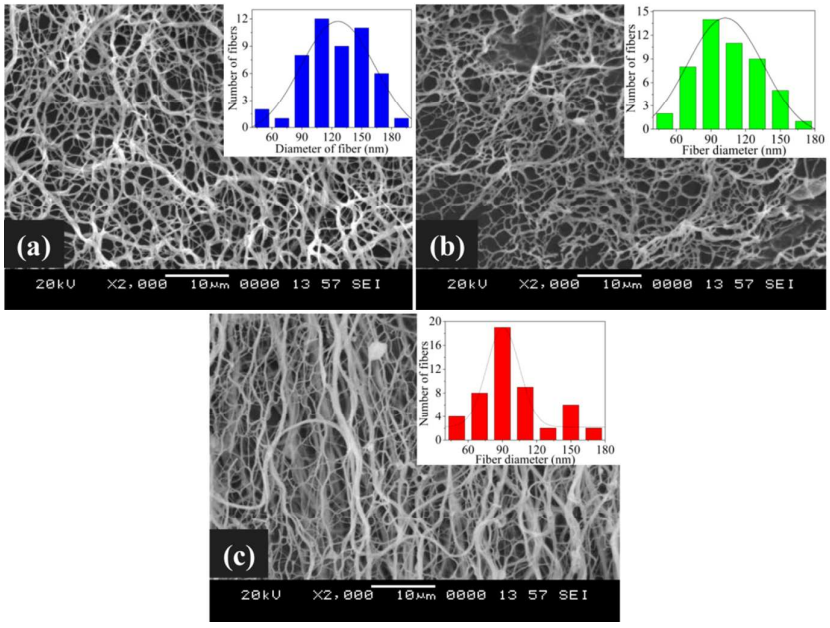

Fig. 3 SEM micrographs of Co_3O_4 nanofibres calcined at (a) 773 K, (b) 873 K and (c) 973 K.

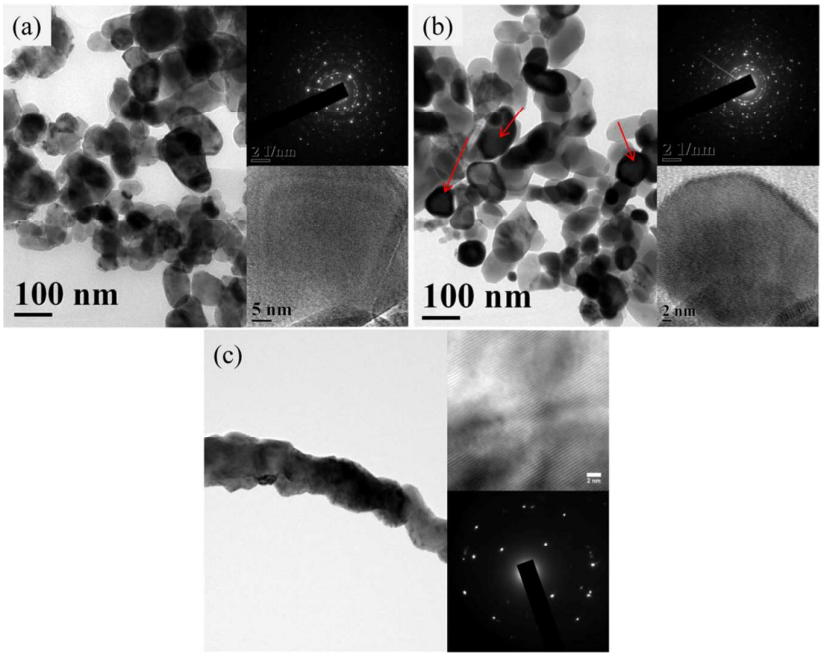

Fig. 4 TEM micrographs of Co_3O_4 nanofibres calcined at (a) 773 K, (b) 873 K and (c) 973 K.

Table 2 EDS results of cobalt oxide obtained at various calcination temperatures

Element	Mass percentage (%)				Atomic percentage (%)			
	773 K	873 K	973 K	theoretical	773 K	873 K	973 K	theoretical
Cobalt	67.97	72.40	73.61	73.42	36.56	41.59	43.09	42.86
Oxygen	32.03	27.60	26.39	26.58	63.44	58.41	56.91	57.14

RSC Advances Accepted Manuscript

The SEM-EDS results of the Co_3O_4 nanofibres obtained by calcining SAN/CATH composite nanofibres at different temperatures are shown in Table 2. The mass and atomic percentages of cobalt and oxygen of the calcined Co_3O_4 nanofibres were compared with their theoretical values in Table 2. The deviation in atomic and mass percentages of the elements increases as the calcination temperature is lowered. When the calcination temperature was 973 K, the theoretical and actual percentages match very closely with each other.

The FTIR spectra of Co_3O_4 nanofibres obtained at different calcination temperatures are shown in Fig. 5a. The peaks at 668 and 574 cm^{-1} confirm the formation of Co_3O_4 nanofibres. It is also noted that there are no peaks representing the organic groups as observed in the case of SAN/CATH, confirming the complete elimination of organic groups from the precursors. Both these bands originate from the metal-oxygen covalent bonds. Co_3O_4 has a spinel structure, the peaks at 668 cm^{-1} and 574 cm^{-1} correspond to the interaction of oxygen with Co^{2+} ions in the tetrahedral hole and Co^{3+} ions in the octahedral hole,[18] respectively.

Table 3 Crystalline parameters, band gap energy, Urbach energy and specific surface area of Co_3O_4 nanofibres calcined at 773 K, 873 K and 973 K.

Calcination temperature (K)	Crystallite size (D) (nm)	Lattice Strain (%)	Band gap (eV)		Urbach energy (eV)	Specific surface area (m^2/g)
			E_{g1}	E_{g2}		
773	19.8	-0.0007	1..35	2.72	0.563	15.65
873	22.3	-0.0005	1.4	2.83	0.107	7.16
973	31.5	0.0002	1.4	2.85	0.081	6.86

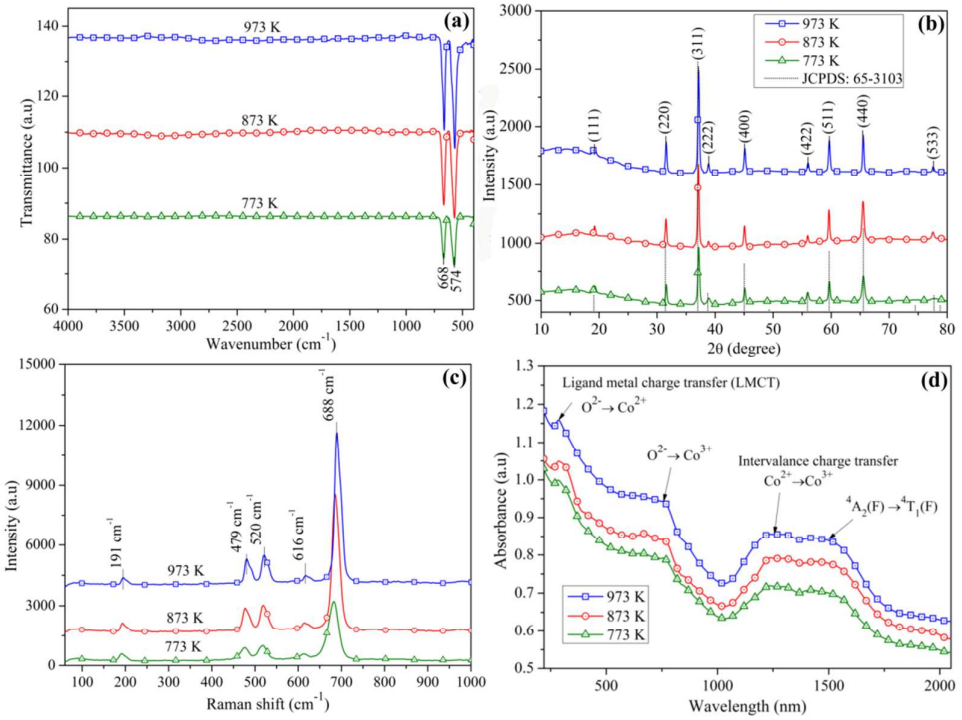

Fig. 5 (a) FTIR spectra, (b) XRD patterns, (c) Raman spectra and (d) UV-Vis-NIR spectra of Co_3O_4 nanofibres obtained at different calcination temperatures

Fig. 5b shows the XRD patterns of the Co_3O_4 nanofibres and the standard JCPDS 65-3103 line diffraction pattern of Co_3O_4. The crystallographic peaks in XRD patterns correspond to Co_3O_4, since all the peaks of the nanofibres exactly match with that of the standard peaks of Co_3O_4 as in Fig. 5b. The sharp peaks of the Co_3O_4 obtained at different calcination temperatures point out the complete elimination of organic phases at the designated temperatures. The obtained Co_3O_4 nanofibres are crystalline in nature. As the calcination temperature is increased an increase in the intensity of the peaks is observed, which is due to the temperature induced grain growth in nanofibres obtained at higher calcination temperatures. The peaks at Bragg angles 19.1, 31.5, 37.1, 38.8, 45.0, 55.9, 59.6, 65.4 and 77.5°, respectively are assigned to (111), (220), (311), (222), (400), (422), (511), (440) and (533) planes of reflection of Co_3O_4. The average crystallite or grain sizes of the Co_3O_4 nanofibres were calculated using the Williamson-Hall method[19] (Fig. S3, ESI†) and their values are presented in Table 3.

The average crystallite size of the fibres increases as a function of the calcination temperature, which is due to the enhanced diffusion of atoms (ions) across the grain boundaries at higher calcination temperatures. The grain growth happens at the expense of smaller grains, because the surface energy of

RSC Advances Accepted Manuscript

 This journal is © The Royal Society of Chemistry 20xx

the smaller grains is higher than that of larger grains. Especially, at the nanoscale, the activation energy of grain growth is in terms of tens of kJ and for bulk it is in terms of hundreds of kJ per mole.[20]

The Raman spectra of the Co_3O_4 nanofibres obtained at different calcination temperatures are shown in Fig. 5c. These spectra were compared with that of a single crystal Co_3O_4 reported elsewhere.[21] For Co_3O_4 with spinel structure and O_h symmetry, the irreducible vibrational modes can be written as,[22]

$$\Gamma = A_{1g} + E_g + 3F_{2g} + 5F_{1u} + 2A_{2u} + 2E_u + 2F_{2u} \quad (1)$$

Among these modes, the A_{1g}, E_g and the three F_{2g} modes are Raman active and the corresponding peaks are at 688, 479, 191, 520 and 616 cm^{-1}, respectively.

The intensities of the Raman peaks increase as a function of the calcination temperature. The Raman peak intensity is in line with the scattering efficiency of a material; therefore, maximum peak intensity is expected for the fibres calcined at 973 K, which has the largest grains as observed in the XRD analysis. A slight shift in the peak position towards higher wavenumbers is also observed as the calcination temperature is increased (Table S2, section 4, ESI†), which is due to the difference in grain size and the associated phonon confinement. The wide peaks observed at low calcination temperature are due to the deviation of composition of cobalt oxide from stoichiometric ratio[23] as observed in the EDS results.

In the diffuse reflectance UV-Vis-NIR spectra of Co_3O_4 nanofibres (Fig. 5d), the absorbance peaks can be assigned to the following transitions; the bands at 1460 and 1220 nm are attributed to crystal field $^4A_2(F) \rightarrow {}^4T_1(F)$ transitions and "intervalence" charge-transfer $Co^{2+} \rightarrow Co^{3+}$, respectively. The absorptions 657 nm and 2788 nm are due to ligand-metal charge transfer events $O^{2-} \rightarrow Co^{3+}$ and $O^{2-} \rightarrow Co^{2+}$, respectively.[24]

The two band gaps i.e., ~1.35 and 2.8 eV, of Co_3O_4 nanofibres corresponds to $O^{2-}(2p) \rightarrow Co^{3+}(e_g)\langle E_{g1}\rangle$ and $O^{2-}(2p) \rightarrow Co^{2+}(t_{2g})\langle E_{g2}\rangle$ transitions.[23,24] (Table 3, Fig. S4a, ESI†). Due to the deviation from the stoichiometric ratio of cobalt and oxygen in the Co_3O_4 nanofibres obtained at different calcination temperature, a slight variation in the band gap energy is observed. The deviation in stoichiometry and the associated change in the band gap energy is estimated with the help of Urbach energy calculations, that is a modification of band gap in the presence of defects due to which the energy of the conduction band decreases and that of the valance band increases.[25,26] In the present case, the narrow band gap of the fibres obtained at 773 K is due to the richness of oxygen[27] in them as observed in EDS analysis. The Urbach energy was calculated by finding out the reciprocal of the slope of the linear region in the plot of *ln(α) vs. hv* (Fig. S4b, ESI†, Table 3). The increase in Urbach energy for the samples with low band gap confirms the postulate on defect-induced reduction in band gap in those samples. The minimum Urbach energy is observed in the case of fibres calcined at 973 K, where the deviation from the stoichiometry of composition is almost negligible. The optical properties of Co_3O_4 are dependent on the grain size of the samples because of the quantum confinement

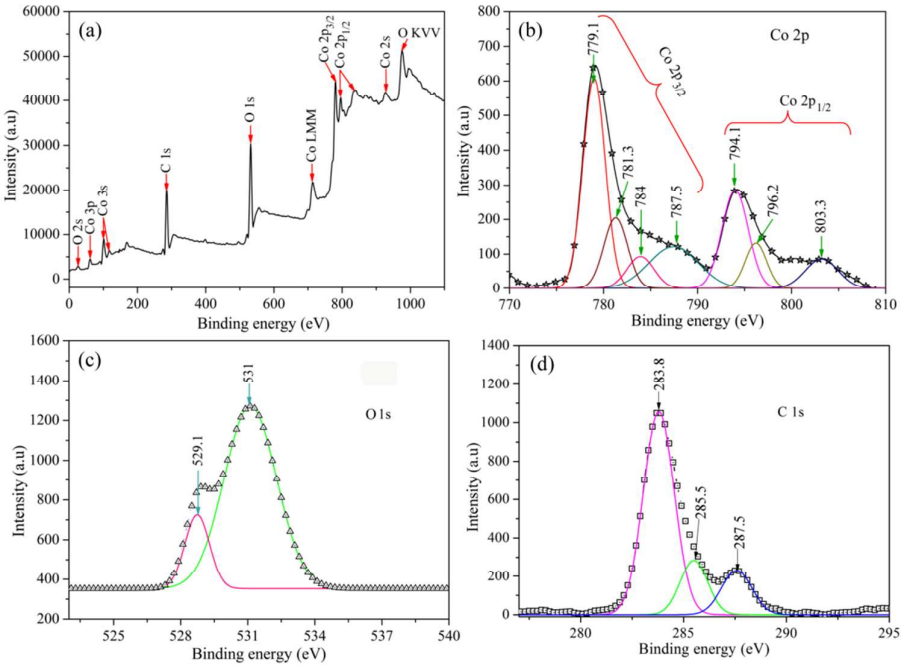

Fig. 6 XP spectra of Co_3O_4 nanofibres calcined at 773 K (a) wide scan, (b) Co 2p, (C) O 1s and (d) C 1s.

The wide scan (0 to 1100 eV) XP spectra of Co_3O_4 nanofibres calcined at 773K is shown in Fig. 6a. The major characteristic peaks are assigned to cobalt (Co 3p, Co 3s, LMM, Co 2p and Co 2s), oxygen (O 1s, KVV) and carbon (C 1s) [28,29]

RSC Advances Accepted Manuscript

and their respective high resolution spectra are shown in Fig. 6b, c & d, respectively.

The peaks at 779.1 and 781.3 eV in the deconvoluted Co 2p spectra are assigned to Co $2p_{3/2}$ of Co^{3+} and Co^{2+}, respectively. Similarly, the peaks at 794.1 and 796.2 eV are attributed to Co $2p_{1/2}$ of Co^{3+} and Co^{2+}, respectively.[30] This, in turn represents the existence of Co^{2+} in the tetrahedral sites and Co^{3+} in the octahedral sites of Co_3O_4. The intermediate peaks are concomitant to the satellite shake up peaks and the gap between Co $2p_{3/2}$-$2p_{1/2}$ peaks are 15±0.1 eV, spin orbit splitting, which corresponds to standard Co_3O_4.[31] In the O 1s spectrum, the peak at 529.1 eV is rising from the lattice oxygen, whereas the more intense one at 531 eV is due to the oxygen defect species or the adsorbed oxygen or the oxygen in other adsorbed species, such as CO_2[31] or the hydroxide groups[32]. In the C 1s spectrum of carbon, the peaks correspond to the adventitious atmospheric carbon, which is inevitable in the calibration. The peaks at 283.8, 285.5 and 287.5 eV can be assigned to C-C, C-O-C and O-C=O, respectively.

The specific surface area of the Co_3O_4 nanofibres calcined at different temperatures is shown in Table 3. An approximately twofold reduction in surface area is observed as the calcination temperature is increased from 773 to 873 K, but, a further rise in the calcination temperature does not bring any substantial change in the surface area. The small grain size and the pores between the grains resulted in the large surface area in the fibres calcined at 773 K. In the case of fibres calcined at 873 K, the subsequent grain growth and the densification in fibres reduced the porosity and thus the surface area. Therefore, it is assumed that, the complete densification of grains take place at around 873 K, thereby, no further remarkable change is observed in the surface area with an increase in the calcination temperature.

Use of Co_3O_4 nanofibres as an electrocatalyst for water splitting

Hydrogen evolution reaction

The hydrogen evolution reaction (HER) catalysed by cobalt oxide nanofibre modified graphite electrode in KOH medium was studied using CV and chrono-potentiometry techniques. CV is a powerful tool to provide considerable information on the thermodynamics of redox processes and the kinetics of heterogeneous electron-transfer reactions and on coupled chemical reactions or adsorption processes. In chrono-potentiometry, a definite current is applied between the auxiliary and working electrodes and the potential of the working electrode (measured with respect to the reference electrode, SCE) is monitored. The basis of controlled current experiments is the redox (electron transfer) reactions that occur at the surface of the working electrode to support the applied current.

For HER, CV was carried out with electrodes containing Co_3O_4 nanofibres calcined at different temperatures, in a potential window of 0.0 V to -1.6 V, for 50 cycles under 1M KOH. The influence of scan rate on the HER efficiency of the modified electrode was tested using Co_3O_4 calcined at 773 K under different scan rates of 10, 50 and 100 mVs^{-1}; the maximum peak current for the stable cycle, obtained after attaining equilibrium, was observed to be at a scan rate of 100 mV s^{-1}. Therefore, all the cyclic voltammograms for cobalt oxide nanofibre modified graphite electrodes were recorded at a scan rate of 100 mV s^{-1}. During the CV analysis for 50 cycles, the peak current at -1.6 V was found to decrease sequentially for a dozen of initial cycles and then become constant. This change in peak current may be due to the progressive resistance induced by the hydrogen bubbles formed on the catalyst surface which stabilized once the equilibrium for the formation and detachment of hydrogen gas is attained. From the CV analysis, the maximum peak current for equilibration of Co_3O_4 nanofibres calcined at 773 K found to be the least (Fig. 7, Table 4). The highest catalytic activity of the Co_3O_4 calcined at 773 K in HER may be attributed to its highest surface area and unique morphology and non-stoichiometry as discussed before.

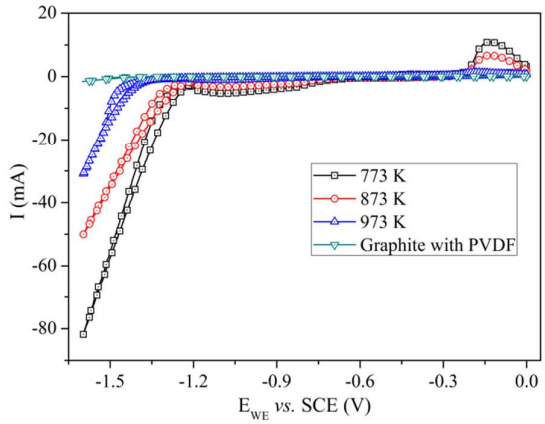

Fig. 7 CV curves for HER studies using electrodes with Co_3O_4 nanofibres calcined at different temperatures.

HER is one of the most intensively studied reaction in electrochemistry due to its simplicity for producing very clean gaseous hydrogen. During HER, protons from the solution combine with electrons at the cathode to form chemisorbed hydrogen atoms at the electrode surface and subsequently to H_2 gas.[33,34]

The chrono-potentiometry study for the evolution of hydrogen on cobalt oxide modified graphite electrode was made at a constant current of -300 mA for a duration of 1800 s. This stable current for H_2 and O_2 evolution was fixed after measuring the amount of H_2 liberated using Co_3O_4 fibres obtained at 773 K at different applied currents (Fig. S5 & S6, ESI†). The electro-catalytic behaviour of each sample prepared at different calcination temperatures was evaluated by measuring the amount of H_2 liberated for the first 300 s. The nature of chrono-potentiograms for each sample are shown in Fig. 8 and the volume of hydrogen liberated on these modified electrodes for the first 300 s are also shown in the inset of Fig. 8. Co_3O_4 nanofibres calcined at 773 K were found to produce the maximum amount of H_2 gas. This observation is a testimony for its best electrocatalytic behaviour for HER in this study.

RSC Advances Accepted Manuscript

This journal is © The Royal Society of Chemistry 20xx

Table 4 The H_2 and O_2 evolution reaction parameters of electro spun cobalt oxide nanofibres developed at different calcination temperature.

Calcination temperature (K)	Cathodic peak current at 1.6 V (mA)	Onset potential of H_2 evolution (E_{WE} vs SCE) (V)	Anodic peak current at 0.75 V (mA)	Onset potential of O_2 evolution (E_{WE} *vs*. SCE) (V)
773	-82.1	-1.26	110.1	0.54
873	-52.2	-1.31	208.4	0.48
973	-33.3	-1.41	358.3	0.43

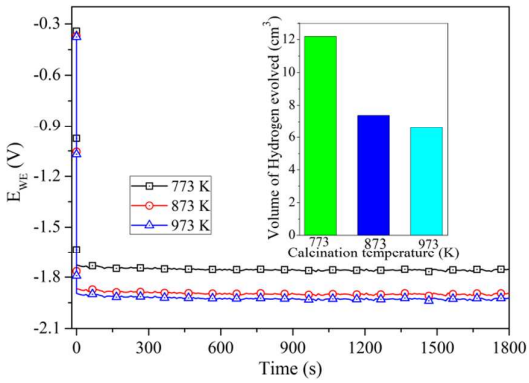

Fig. 8 Chrono-potentiometry study for evolution of hydrogen using Co_3O_4 nanofibres calcined at different temperatures and the respective evolution of H2 after 300s, in the inset.

Oxygen evolution reaction

The Co_3O_4 nanofibres calcined at different temperatures were also tested for their electro-catalytic activity in oxygen evolution reaction (OER) in 1 M KOH, in the same line as HER.

The CV experiments for OER on Co_3O_4 nanofibre modified graphite electrodes were conducted in the potential range of 0 to 0.75 V at a scan rate of 100 mV s^{-1}. The onset potential for continuous evolution of O_2 gas was found from the CV curves. It is observed that the sample calcined at 973 K is showing the maximum catalytic activity towards OER with the lowest onset potential (0.43 V) (Fig. 9, Table 4).

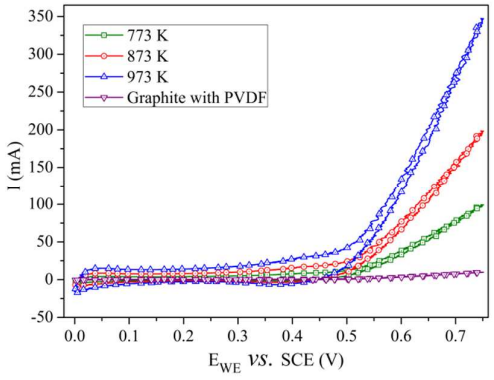

Fig. 10 CV curves for OER studies using electrodes with Co_3O_4 nanofibres calcined at different temperature.

The efficiency of electroactive cobalt oxide nanofibres for OER was also studied using chrono-potentiometry. The amount of oxygen evolved was measured in the similar way as discussed for HER and the corresponding chrono-potentiogram is shown in Fig. 10. As the current pulse of +300 mA was applied, a sharp increase in the potential was observed until a potential at which OH^- is oxidized to O_2 is reached. Once equilibrium is attained between the newly forming bubbles and that escaping from the surface of the electrode, the potential is found to be stable throughout the experiment with continuous evolution of oxygen. The inset in Fig. 10 shows the relative amount of O_2 liberated in 300s on Co_3O_4 nanofibres calcined at different temperatures. In this case, the Co_3O_4 nanofibres calcined at 973 K exhibit the least potential for O_2 evolution and hence they are the most effective electroactive material for OER.

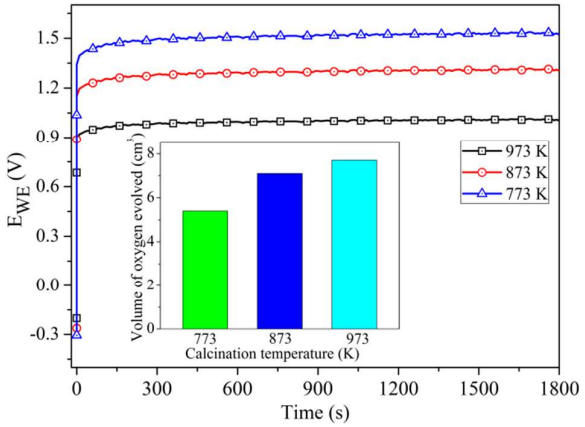

Fig. 10 Chrono-potentiometry study for evolution of oxygen using Co_3O_4 nanofibres calcined at different temperatures and the respective evolution of O_2 after 300s, in the inset.

The results of this study reveal that the Co_3O_4 nanofibres calcined at 773 K exhibit the maximum efficiency towards H^+ ion adsorption and thereby the highest catalytic activity towards HER. At the same time, it is a very weak material towards OER due to its poor efficiency towards OH^- adsorption. Contrarily, the sample calcined at 973 K exhibit the maximum catalytic efficiency in OER due its higher surface activity towards OH^- adsorption. It may be inferred that the surface favouring the cathodic reaction has an adverse effect on the anodic reaction and vice versa.

Conclusions

The SAN/CATH precursor composite fibres with the smallest average fibre diameter were obtained at an applied voltage of 22 kV, tip to collector distance of 17 cm, solution flow rate of 1000 µL.h^{-1} and a solution concentration of 20 w/v %. The Co_3O_4 nanofibre diameters were reduced significantly after calcination, as compared with that of the SAN/CATH composite fibres. The Co_3O_4 nanofibres were composed of

RSC Advances Accepted Manuscript

sintered grains as observed in the TEM results and the dense packing of these grains at the maximum calcination temperature lead to a significant reduction in surface area. The grain sizes increased with an increase in the calcination temperature, which is revealed by the Raman and XRD results. The presence of defects in these fibres made a difference in their band gap energies and the amount of defects decreased as the calcination temperature was increased. The XPS analysis showed that the spectrum was typically that of Co_3O_4. The Co_3O_4 nanofibres were efficient in the water splitting reaction. In summary, it may be concluded that among the Co_3O_4 nanofibres calcined at three different temperatures, the ones calcined at 773 K and 973K exhibited the highest electrocatalytic activity in water splitting of HER and OER, respectively in 1 M KOH solution.

Acknowledgement

G.G. would like to thank the dept. of Metallurgical and Materials Engg., National Institute of Technology of Karnataka (NITK), India for a research fellowship. The authors thank Ms. U. Rashmi and Ms. Akshata G. Patil for their kind assistance in scanning electron microscopy and X-ray diffraction, respectively. Authors would like to thank Mr. S. Varadharaja Perumal, CENSE, IISc, Bangalore for the XPS studies. The authors also thank Dr. I. Regupathi dept. of Chemical engineering, National Institute of Technology of Karnataka (NITK) for the TGA facility.

References

1 M. E. Lyons, *Int. J. Electrochem. Sci.*, 2008, **3**, 1425 – 1462.
2 Y. Yamada, K. Yano, Q. Xu and S. Fukuzumi, *J. Phys. Chem. C*, 2010, **114**, 16456–16462.
3 D. Brown, M. Mahmood, M. Man and A. Turner, *Electrochim. Acta*, 1984, **29**, 1551–1556.
4 P. Du, L. Song, J. Xiong, N. Li, Z. Xi, L. Wang, D. Jin, S. Guo, Y. Yuan, *Electrochim. Acta*, 2012, **78,** 392–397.
5 G. George and S. Anandhan, *J. Sol-Gel Sci. Technol*., 2013, **67** () 256–266.
6 G. Wang, H. Wang, Y. Ling, Y. Tang, X. Yang, R. C. Fitzmorris, C. Wang, J. Z. Zhang and Y. Li, *Nano lett.*, 2011, **11**, 3026–3033.
7 X.-Y. Zhang, H.-P. Li, X.-L. Cui and Y. Lin, *J. Mater. Chem.*, 2010, **20**, 2801–2806.
8 X. Yang, A. Wolcott, G. Wang, A. Sobo, R. C. Fitzmorris, F. Qian, J. Z. Zhang and Y. Li, *Nano Lett.*, 2009, **9**, 2331–2336.
9 K. Sivula, R. Zboril, F. Le Formal, R. Robert, A. Weidenkaff, J. Tucek, J. Frydrych and M. Gratzel, *JACS*, 2010, **132**, 7436–7444.
10 Y. Lee, J. Suntivich, K. J. May, E. E. Perry and Y. Shao-Horn, *J. Phys. Chem. Lett.*, 2012, **3**, 399–404.
11 B. S. Yeo and A. T. Bell, *JACS*, 2011, **133**, 5587–5593.
12 J. Gaudet, A. Tavares, S. Trasatti and D. Guay, *Chem. Mater.*, 2005, **17**, 1570–1579.
13 G. Marras, M. Artal, S. Otin and B. Marongiu, *Fluid Phase Equilib*., 1994, **98**, 149–162.
14 T. Senthil and S. Anandhan, *J. Elastomers Plast*., 2013, DOI: 10.1177/0095244313514987
15 W.S Rasband, ImageJ 1.48, U. S. National Institutes of Health, Bethesda, Maryland, USA, http://imagej.nih.gov/ij/ (1997-2014).
16 J. Scheirs, *Practical polymer analysis: techniques and strategies for the compositional and failure analysis of polymers, elastomers and composites*, Wiley, New York, 2000.
17 T. Wanjun and C. Donghua, *Chem. Pap*., 2007, **61,** 329–332.
18 C.-W. Tang, C.-B. Wang and S.-H. Chien, *Thermochim. Acta*. 2008. **473**, 68–73.
19 A. Khorsand Zak, W.H. Abd. Majid, M.E. Abrishami and R. Yousefi, *Solid State Sci*. 2011, **13,** 251–256.
20 S.-W. Choi, J.Y. Park and S.S. Kim, Mater. *Chem. Phys.* 2011, **127**, 16–20.
21 V.G. Hadjiev, M.N. Iliev and I.V. Vergilov, *J. Phys. C*. 1988, **21,** L199.
22 C.Y. Xu, P.X. Zhang and L. Yan, *J. Raman Spectrosc*., 2001, **32**, 862–865.
23 D. Barreca, C. Massignan, S. Daolio, M. Fabrizio, C. Piccirillo, L. Armelao and E. Tondello, *Chem. Mater*. 2001, **13**, 588–593.
24 Y. Zhang, Y. Chen, T. Wang, J. Zhou and Y. Zhao, *Micropor. Mesopor. Mater*. 2008, **114**, 257–261.
25 B. Choudhury, M. Dey and A. Choudhury, *Int. Nano. Lett*. 2013, **3**, 1–8.
26 K. Boubaker, *Eur. Phys. J. Plus*. 2011, **126**, 1–4.
27 I. Justicia, P. Ordejón, G. Canto, J.l. Mozos, J. Fraxedas, G.A. Battiston, R. Gerbasi and A. Figueras, *Adv. Mater*. 2002, **14**, 1399–1402.
28 A. G. Kochur, T. M. Ivanova, A. V. Shchukarev, R. V. Linko, N. G. Terebova, A. A. Sidorov and I. L. Eremenko, *Russ. J. Inorg. Chem.*, 2011, **56**, 402–408.
29 Y. Fan, N. Zhang, L. Zhang, H. Shao, J. Wang, J. Zhang and C. Cao, *J. Electrochem. Soc.*, 2013, **160**, F218–F223.
30 N. S. McIntyre and M. G. Cook, *Anal. Chem.*, 1975, **47**, 2208–2213.
31 D. Briggs and V. Gibson, *Chem. Phys. Lett.*, 1974, **25**, 493–496.
32 S. C. Petitto, E. M. Marsh, G. A. Carson and M. A. Langell, *J. Mol. Catal. A: Chem.*, 2008, **281**, 49–58.
33 J. Kubisztal and A. Budniok, *Int. J. Hydrogen Energy*, 2008, **33**, 4488–4494.
34 Y. Ullal and A. C. Hegde, *Int. J. Hydrogen Energy*, 2014, **39**, 10485–10492.

RSC Advances Accepted Manuscript

 This journal is © The Royal Society of Chemistry 20xx

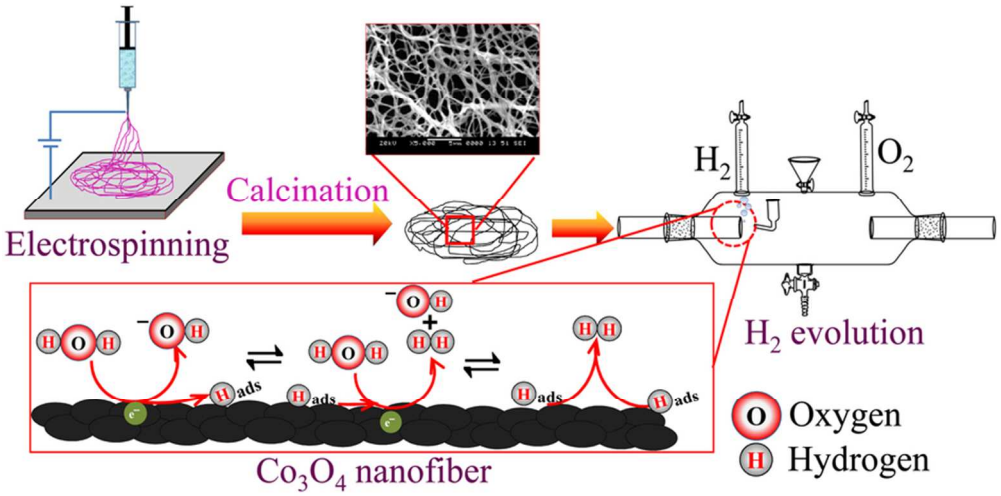

40x20mm (600 x 600 DPI)

RSC Advances Accepted Manuscript